Experimental and Numerical Investigation of the Equilibrium Geometry of Liquid Lenses

J. C. Burton,*[†,‡] F. M. Huisman,[†] P. Alison,[†] D. Rogerson,[†] and P. Taborek[†]

[†]*Department of Physics and Astronomy, University of California, Irvine, Irvine, California 92697.*
[‡]*Current address: James Franck Institute, The University of Chicago, Chicago, Illinois 60637.*

The equilibrium configuration of a nonwetted three fluid system takes the form of a floating liquid lens, where the lens resides between an upper and lower phase. The axisymmetric profiles of the three interfaces can be computed by solving the nonlinear Young−Laplace differential equation for each interface with coupled boundary conditions at the contact line. Here we describe a numerical method applicable to sessile or pendant lenses and provide a free, downloadable *Mathematica Player* file which uses a graphical interface for analyzing and plotting lens profiles. The results of the calculations were compared to optical photographs of various liquid lens systems which were analyzed using basic ray-tracing and Moiré imaging. The lens profile calculator, together with a measurement of the lens radius for a known volume, provides a simple and convenient method of determining the spreading coefficient (*S*) of a liquid lens system if all other fluid parameters are known. If surfactants are present, the subphase surface tension must also be self-consistently determined. A procedure is described for extracting characteristic features in the optical images to uniquely determine both parameters. The method gave good agreement with literature values for pure fluids such as alkanes on water and also for systems with a surfactant (hexadecane/DTAB), which show a transition from partial wetting to the pseudopartial wetting regime. Our technique is the analog of axisymmetric drop shape analysis, applied to a three fluid system.

Introduction

When a drop of liquid is placed on the quiescent surface of an immiscible fluid, its final shape depends on the relative values of the various surface tensions and whether the liquids wet each other. A wetting droplet will spread out into an expanded film of near-molecular thickness (complete wetting, Figure 1c), while a nonwetting droplet will spread to a finite size and form a liquid lens on the surface (partial wetting, Figure 1a). The latter is the case for many common organic liquid systems, such as heavy alkanes on water. In this Article, we are concerned with the equilibrium geometry of these liquid lenses under the influence of surface tension and gravity. The static geometry of such a system will depend on the mass density of the lens, the subfluid phase, and the surrounding gas as well as three surface tensions associated with three separate interfaces. These interfaces can be seen in Figure 2, which shows a typical profile of a liquid lens. In principle, a three-phase contact line such as that in Figure 2 is also characterized by an associated line tension. For liquid lens systems, recent experiments and theory[1−4] have shown that the magnitude of the line tension is negligibly small, so we will ignore this in our analysis. Brochard-Wyart et al.[5] showed that the wetting conditions can also depend on the relative Hamaker constants of the liquids. For certain values of the parameters,

a finite liquid lens can exist in equilibrium with a thin wetting film (Figure 1b), which is known as the pseudopartial wetting regime. However, on macroscopic scales, this situation can be modeled as having an effective surface tension for the subphase fluid, and will be treated as such in this work.

There are two limits in which an analytic treatment of these systems is possible. For very small lenses where the effects of gravity can be ignored, the interfaces of the lens take the form of spherical caps, and the surface of the subfluid is perfectly flat. In the opposite case of very large lenses, the shape is that of a flat "pancake", that is, a nearly perfect cylindrical disk. This limit, in which the thickness of the disk is independent of the volume, was first discussed by Langmuir in 1933[6] and subsequently by Scriven and Huh in 1972.[7] For intermediate cases, typically corresponding to lenses with a diameter of a few millimeters to a few centimeters, the shape of the interfaces depends on the volume of the lens and must be found by solving the axisymmetric Young−Laplace equation:

$$\Delta P = 2\kappa_m \sigma - \Delta\rho gz \tag{1}$$

where $\Delta P = P_{in} - P_{out}$ is the pressure difference between the interior and exterior fluid, κ_m is the mean curvature of the interface, σ is the surface tension at the relevant interface, $\Delta\rho = \rho_{in} - \rho_{out}$ is the density difference between the fluids, g is the gravitational acceleration, and z is the axial position of the interface (cf. Figure 2). Equation 1 is a nonlinear differential equation because the curvature term contains products of derivatives of the surface profile. Some solutions and configurations have been presented by previous authors.[7−10] Computation of

*To whom correspondence should be addressed. E-mail: jcburton@uchicago.edu.

(1) Aveyard, R.; Cline, J. H.; Nees, D.; Paunov, V. *Colloids Surf., A* **1999**, *146*, 95–111.
(2) Amirfazli, A.; Neumann, A. W. *Adv. Colloid Interface Sci.* **2004**, *110*, 121–141.
(3) Schimmele, L.; Napïrkowski, M.; Dietrich, S. *J. Chem. Phys.* **2007**, *127*, 164715.
(4) Takata, Y.; Matsubara, H.; Matsuda, T.; Kikuchi, Y.; Takiue, T.; Law, B.; Aratono, M. *Colloid Polym. Sci.* **2008**, *286*, 647–654.
(5) Brochard-Wyart, F.; di Meglio, J. M.; Quere, D.; de Gennes, P. G. *Langmuir* **1991**, *7*, 335–338.

(6) Langmuir, I. *J. Chem. Phys.* **1933**, *1*, 756–776.
(7) Huh, C.; Scriven, L. E. *J. Colloid Interface Sci.* **1972**, *40*, 82–98.
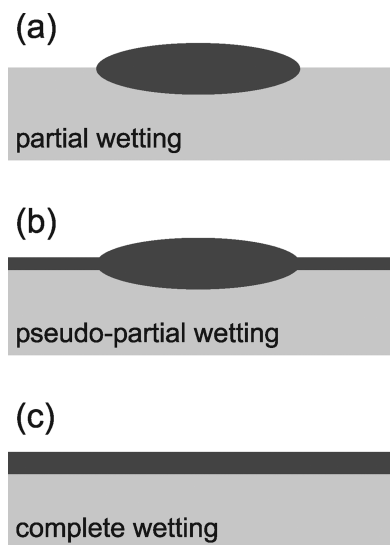(8) Princen, H. M. *J. Colloid Sci.* **1963**, *18*, 178–195.

Published on Web 09/01/2010

Figure 1. Three possible wetting conditions for a three fluid system. (a) The partial wetting regime is characterized by a liquid lens of finite size and contact angle. (b) In the pseudopartial wetting regime, macroscopic lenses can exist in equilibrium with a thin wetting film, typically only tens of nanometers thick. (c) In a completely wetted system, the surfaces are flat and the upper fluid completely covers the subphase fluid.
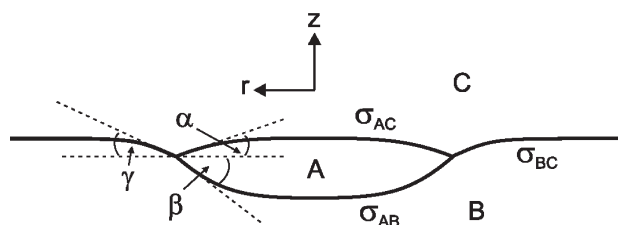

Figure 2. Cartoon of a generic liquid lens (A) floating on a subfluid phase (B) surrounded by vapor (C). The contact angles α, β, and γ are defined from the horizontal. Each phase has a mass density (ρ_A, ρ_B, ρ_C), and to guarantee gravitational stability we require $\rho_C < \rho_A < \rho_B$. Each interface is described by a surface tension σ_{xy}, where xy denotes the A/B, A/C, or B/C interface.

lens shapes requires an iterative numerical solution of eq 1 for each interface, together with rather complicated matching conditions at the contact line. We have numerically computed the shapes of various hydrocarbon lenses floating on the surface of water surrounded by air for a wide range of lens parameters (surface tension, density, volume, etc.) and compared the results to experimental values. The simplest experimental parameters to measure and control are the lens volume and radius; the most difficult parameter to determine experimentally is the hydrocarbon/water interfacial tension or, equivalently, the spreading parameter $S = \sigma_{BC} - \sigma_{AB} - \sigma_{AC}$. Equation 1 implicitly determines a relationship between these quantities; that is, for given values of the fluid/air interfacial tensions, spreading coefficient, densities, and the radius of a lens, there is a unique value of the lens volume consistent with hydrostatic equilibrium. Initially, we computed the shapes of thousands of different combinations of lens parameters and tried to use the results to determine a high order polynomial fitting function to provide an explicit relation between the geometrical parameters of the lens and the spreading

parameter S. This method turned out to be quite cumbersome and prone to error. Instead, we developed, a free, graphical interface for computing lens profiles as a *Mathematica Player* file, which is available for download via the Supporting Information. Using the provided lens profiler together with easily determined fluid properties, S can be conveniently estimated with little error over a wide range of physical parameters.

The radius and volume are two particularly simple geometric characteristics of a lens, but the solutions to eq 1 provide the entire shape, including the spatial variation of the curvature. Another goal of this Article is to compare experimental measurements of the geometry of liquid lens systems to the equilibrium shapes computed from the Young−Laplace equation. Our initial motivation and interest in this problem was to understand the relationship between the optical signatures of static liquid lenses and their geometry, and to eventually apply this to previous work in our lab, in which liquid lenses undergo dynamic pinch-off and produce a fractal-like pattern of satellite droplets.[11] The current experiment consists of measuring the convergence of incident, parallel, monochromatic light after passing through a liquid lens at various distances from the surface of the subfluid. The liquid lens can be considered an optical lens where the exact details of the surface profile are unknown. We compare experiment and theory by tracing light rays through computed lens shapes (using eq 1); by adjusting the surface tensions used as inputs into the calculation, good agreement was obtained for all of the fluids used in our experiment. Surface deformations of the subfluid phase are rather small and are difficult to measure quantitatively using ray tracing. Moiré imaging is ideally suited to measuring small angular variations in a surface; we used this technique to directly measure the subfluid contact angle γ in Figure 2, which is typically only a few degrees. Finally, we illustrate the applicability of our method to lens systems with the addition of a cationic surfactant, dodecyltrimethylammonium bromide (DTAB), to the water subphase with a hexadecane lens resting on the surface. This system is known to have a pseudopartial wetting transition, characterized by a minimum in the dihedral angle subtended by the lens as a function of surfactant concentration.[12,13] Using our method, we have simultaneously measured the spreading coefficient, contact angles, and subphase surface tension in the presence of a hexadecane lens, which is in good agreement with similar measurements reported in refs 12 and 13.

Numerical Method

The geometry under consideration is that of an axisymmetric liquid lens phase A of density ρ_A floating on a subfluid phase B of density ρ_B. Above both the lens and the subphase, there is a vapor (or liquid) phase C of density ρ_C. The interfaces between the liquids have surface tensions denoted by σ_{AC}, σ_{BC}, and σ_{AB} (Figure 2). For our discussion, we will assume that $\rho_C < \rho_A < \rho_B$, which is sufficient (but not necessary) to guarantee gravitational stability for all lenses regardless of size. The subfluid extends radially in a cylindrical container of radius Σ with a boundary condition of 90° contact angle on the wall. As long as the distance from the edge of the lens to the wall of the container is much greater than the capillary length of the subfluid phase ($\Sigma - R \gg [\sigma_{BC}/g(\rho_B - \rho_C)]^{1/2}$), then deformations of the subfluid interface will not affect the shape of the surface near the wall. In this case, the system provides a good approximation to a lens floating on an infinite subfluid phase. The shape of the axisymmetric

(9) Ross, D. S. *J. Colloid Sci.* **1992**, *154*, 66–76.
(10) Cabezas, M. G. G.; Bateni, A.; Montanero, J. M.; Neumann, A. W. *Langmuir* **2006**, *22*, 10053–10060.

(11) Burton, J. C.; Taborek, P. *Phys. Rev. Lett.* **2007**, *98*, 224502.
(12) Matsubara, H.; Ikeda, N.; Takiue, T.; Aratono, M.; Bain, C. D. *Langmuir* **2003**, *19*, 2249–2253.
(13) Wilkinson, K. M.; Bain, C. D.; Matsubara, H.; Aratono, M. *Chem. Phys. Chem.* **2005**, *6*, 547–55.

fluid interfaces can be described using parametric polar coordinates $(r(j), z(j))$ with a constant differential arclength

$$dl = \sqrt{\left[r'(j)^2 + z'(j)^2 \right]} \ dj = L \ dj \ \text{ and } 0 \leq j \leq 1$$

For each separate interface, the point $j = 0$ always corresponds to where the slope of the interface is zero (i.e., the top and bottom of the lens and the intersection of the subphase with the container wall). The point $j = 1$ always corresponds to the intersection of the three interfaces (contact line). In this formulation, the total arclength in the $r - z$ plane is $\int_0^1 [r'(j)^2 + z'(j)^2]^{1/2} \ dj = L$ (L will of course be different for each interface). Using these parametric coordinates, the expression for the mean curvature term in eq 1 is

$$\kappa_m = \frac{1}{2} \left(\frac{z'(j)}{r(j)\sqrt{r'(j)^2 + z'(j)^2}} + \frac{r'(j)z''(j) - z'(j)r''(j)}{(r'(j)^2 + z'(j)^2)^{3/2}} \right) \quad (2)$$

Equation 1 provides one relation between the unknown functions $r(j)$ and $z(j)$; the arclength parametrization $dl/dj = L$ provides another. The equations can be made dimensionless by the radius of the lens R, the surface tension σ of the interface, and the density difference $\Delta\rho = \rho_{in} - \rho_{out}$ across the interface, where ρ_{in} denotes the high pressure side. The resulting coupled differential equations can be written as

$$\tilde{r}''(j) = \tilde{z}'(j) \left(2\tilde{L}\tilde{P} - \tilde{L}B_o\tilde{z}(j) + \frac{\tilde{z}'(j)}{\tilde{r}(j)} \right) \quad (3)$$

$$\tilde{z}''(j) = -\tilde{r}'(j) \left(2\tilde{L}\tilde{P} - \tilde{L}B_o\tilde{z}(j) + \frac{\tilde{z}'(j)}{\tilde{r}(j)} \right) \quad (4)$$

where $\tilde{r} = r/R$, $\tilde{z} = z/R$, $\tilde{L} = L/R$, $\tilde{P} = \Delta P R/(2\sigma)$, and $B_o = \Delta\rho g R^2/\sigma$ is the gravitational Bond number. The constant ΔP is the pressure difference across the surface at $(r,z) = (0,0)$ for the lens interfaces (AB and AC), and $(r,z) = (\Sigma,0)$ for the BC interface. There will be different values of $\tilde{P}$ and $\tilde{L}$ for each interface. Since the shape of the interface is independent of the absolute axial position z, we have lost no generality by assuming that $z(0) = 0$ as one of the initial conditions to the equations, and the interfaces are to be translated vertically after computation. To compute the shape of a liquid lens system we must solve eqs 3 and 4 subject to boundary conditions on the contact angles discussed below; the equations must be solved three times, once for each interface. This is accomplished by solving a sequence of initial value problems using a shooting method to satisfy the boundary conditions. To obtain a well posed initial value problem, a guess for the arc length parameter L and the pressure difference ΔP must be provided, so for the three interfaces there is a total of six parameters. There are also six boundary conditions which uniquely determine the parameters. Three boundary conditions come from the requirement that the three interfaces meet to form a three-phase contact line with $r(j) = R$ at $j = 1$, or in reduced variables:

$$\tilde{r}(1) = 1 \quad (5)$$

The interfaces meet at angles defined by

$$|\tilde{z}'(1)/\tilde{r}'(1)| = \tan(\theta_c) \quad (6)$$

where θ_c corresponds to α, β, or γ as shown in Figure 2, depending on the interface being considered. The three contact angles are not independent, however, and must satisfy a force balance in the r and z directions at the contact line:

$$\sigma_{AC} \cos(\alpha) + \sigma_{AB} \cos(\beta) - \sigma_{BC} \cos(\gamma) = 0 \quad (7)$$

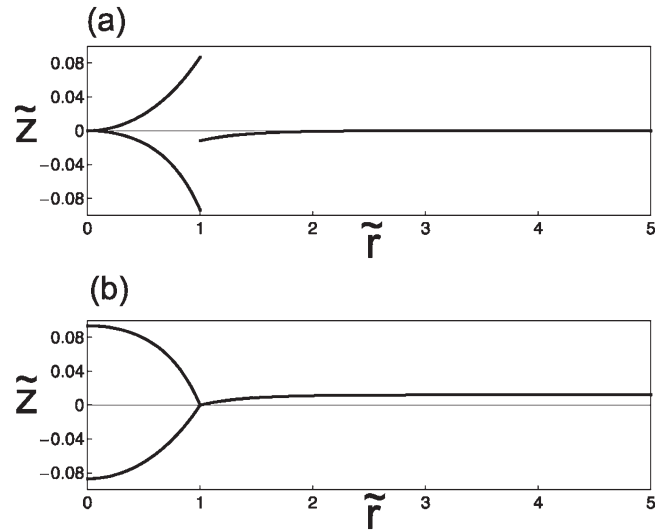$$\sigma_{AC} \sin(\alpha) - \sigma_{AB} \sin(\beta) + \sigma_{BC} \sin(\gamma) = 0$$

Figure 3. (a) Solutions of eqs 3 and 4 for each interface of the lens. The two curves that describe the lens interface start at $(\tilde{r}(0), \tilde{z}(0)) = (0,0)$, while the interface of the subfluid begins at $(\tilde{r}(0), \tilde{z}(0)) = (\tilde{\Sigma},0)$. Each interface is then numerically integrated to the contact line at $\tilde{r}(1) = 1$. (b) The interfaces are then translated vertically so that all three match at the contact line where $\tilde{z} = 0$.

which provides two additional boundary conditions. The final boundary condition comes from the requirement that the pressure drop around a closed loop that encloses the three-phase contact line must vanish:

$$\sigma_{AC}\kappa_{AC} - \sigma_{AB}\kappa_{AB} - \sigma_{BC}\kappa_{BC} = 0 \quad (8)$$

where κ_{xy} is the mean curvature of the given interface at the contact line. Mathematically, eq 7 imposes a condition on the first derivatives ($\tilde{z}'(j)$ and $\tilde{r}'(j)$), while eq 8 imposes a condition on the second derivatives ($\tilde{z}''(j)$ and $\tilde{r}''(j)$). The numerical procedure consists of constructing an initial guess for ΔP and L, or equivalently $\tilde{P}$ and $\tilde{L}$, and propagating the solution of eqs 3 and 4 from $j = 0$ to $j = 1$ with the initial conditions $z(0) = 0$, $z'(0) = 0$, $r(0) = 0$, and $r'(0) = \tilde{L}$ for the lens interfaces (AB and AC), and $z(0) = 0$, $z'(0) = 0$, $r(0) = \Sigma$, and $r'(0) = \tilde{L}$ for the BC interface using the *Mathematica* NDSolve function. The appropriate values of the $\tilde{P}$ and $\tilde{L}$ parameters which generate solutions which satisfy the boundary conditions eqs 5, 7, and 8 are determined to within a tolerance of 10^{-8} using the *Mathematica* FindRoot function.

With this formulation, the shape of a given liquid lens system is defined using only R, ρ_A, ρ_B, ρ_C, σ_{AC}, σ_{AB}, and σ_{BC}. One could also use the volume of the lens V instead of the radius R to define the system; however, using R is more amendable to the numerical techniques since it enters the equations as a boundary condition rather than an integral conservation law. Although not discussed here, we note that the shapes of pendant lenses can also be calculated using this formulation, which is not possible using other formulations such as those where the angle of declination ϕ is used as the parametric variable;[7,9] in these cases, the functions $r(\phi)$ and $z(\phi)$ can be multivalued.

Figure 3a illustrates our method. The three interfaces are calculated quickly and efficiently using eqs 3 and 4 with the coupled boundary conditions eqs 5, 7, and 8; the three interfaces are then translated vertically to form the lens system, as shown in Figure 3b. The total computation time for one lens system is about $1-2$ s on a 3 GHz computer. Because eqs 3 and 4 are in parametric form, we can calculate the shape of lenses with arbitrary contact angles, ranging from relatively flat pancakes to thick, reentrant liquid lenses. Figure 4 shows examples of these two cases, together with their associated parameters (surface tensions, densities, etc.). In order to provide a quick and efficient way to apply this method for research, we developed a free *Mathematica Player* file with a
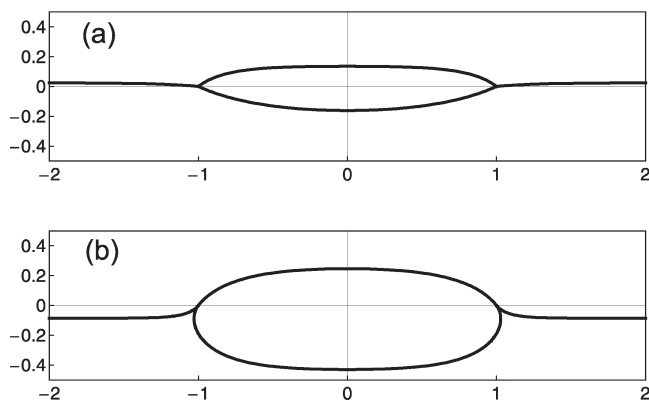
Figure 4. Computed profiles of two floating lenses. Units on both axes are centimeters. (a) Relatively flat (small contact angles) liquid lens system, typical of a hydrocarbon on water. The parameters for this system are $R = 1.0$ cm, $\rho_o = 0.7$ g/cm^3, $\rho_w = 1.0$ g/cm^3, $\sigma_{AC} = 25$ g/s^2, $\sigma_{BC} = 70$ g/s^2, $\sigma_{AB} = 55$ g/s^2, and the volume of the lens is $V = 0.579$ cm^3. (b) Reentrant liquid lens system, typical of water floating on a dense, hydrophobic subphase. The parameters for this system are $R = 1.0$ cm, $\rho_o = 1.0$ g/cm^3, $\rho_w = 2.0$ g/cm^3, $\sigma_{AC} = 70$ g/s^2, $\sigma_{BC} = 20$ g/s^2, $\sigma_{AB} = 50$ g/s^2, and the volume of the lens is $V = 1.639$ cm^3.

graphical user interface. The user enters the relevant fluid properties and can then plot the shapes of the lens and subphase interfaces, as well as find the contact angles and lens volume for a given input radius. If the user wished to measure the spreading coefficient S of a liquid lens system and was confident of the values of σ_{BC} and σ_{AC}, the user would guess values for S until the computed lens volume matched the measured experimental volume. Figure 5 shows a snapshot of the graphical interface for the *Mathematica Player* file. This file is included in the Supporting Information, as well as a full *Mathematica* notebook file that allows for exporting data points along the lens interface. The details of the shape of the lens are required for the ray tracing procedure described below.

Experimental Methods

Lenses of heavy mineral oil, hexadecane, tetradecane, dodecane, and nonane on water were studied using shadowgraphy and Moiré imaging. Shadowgraphy was used primarily to determine the shape of the hydrocarbon lens, while Moiré imaging provided information about the curvature of the water near the contact line. The mineral oil was purchased from Fisher, while the alkanes (99+% pure) were obtained from Sigma-Aldrich. For experiments where a surfactant was purposely introduced, we used dodecyltrimethylammonium bromide (DTAB) obtained from Sigma-Aldrich, which was listed as 99% pure. The values for surface tensions of the fluid/air interfaces, densities, and indices of refraction for each fluid at 25 °C were obtained from a chemical reference database,[14] except in the case of mineral oil. The mineral oil density and index of refraction used were those listed under the heavy mineral oil CAS number at Sigma-Aldrich. Due to variations between lots of mineral oil, we measured the surface tension directly using axisymmetric drop shape analysis. By taking a photograph of a pendant drop of fluid in air, the same numerical process discussed previously can be used to calculate theoretical interfacial shapes. The best fit shape was calculated by manually picking points along the boundary of a pendant drop in a digital photograph and then solving eqs 3 and 4 for the interfacial profile. The resulting profile was then translated and rotated to best fit onto the data points. The rotation and translation corrects for slight tilts in the photographs and linear shifts in the origin of the system. The surface tension and contact angle were adjustable parameters in order to produce the best fit curve to the data.

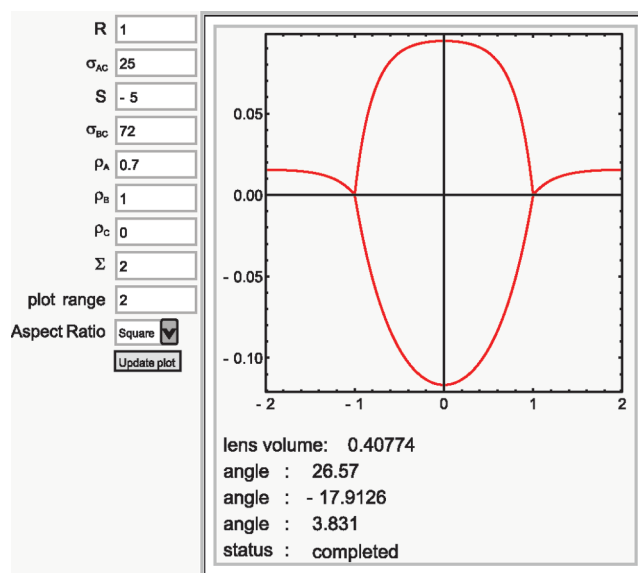(14) Yaws, C. L. *Chemical Properties Handbook*; McGraw-Hill: New York, 1999.

Figure 5. Graphical interface of the lens profiler provided in the Supporting Information. The user enters the fluid parameters, and the lens profiler reports the shape, angles, and volume of the resulting lens system. The full *Mathematica* version also provided allows the user to export data for the coordinates of the lens and subphase shape.

Our criterion for best fit was to minimize the sum of the distance between each point and its corresponding nearest point on the calculated profile. The asymptotic standard error associated with the 95% confidence interval using this technique was typically 0.4 dyn/cm. An example of this method applied to a drop of pure water is shown in Figure 6.

Reproducible results could only be obtained by filtering the alkanes at least once through a column of alumina powder to remove polar impurities, as described in previous studies.[15] The tetradecane was especially impure and exhibited partial to complete wetting behavior when unfiltered, so it was filtered twice, which was sufficient to achieve consistent results. The filtering procedure was not sufficient for hexadecane, so this fluid was vacuum distilled in addition to being filtered. The purified fluids had noticeably different lens geometries than the as-received products, even though the as-received products were at minimum 99% pure. This is to be expected since even small amounts of surfactants and/or impurities can significantly affect the surface tension. Purity is especially critical in liquid lens systems; for example, a system composed of hexadecane lenses floating on aqueous solutions of the surfactant DTAB shows a partial-wetting transition at concentrations of DTAB where the bulk surface tensions have changed by less than 1%.[12,13] This is due to the fact that the surfactant can stabilize an oil layer on the surface of the aqueous phase, usually only 1−10 nm thick, and this layer significantly reduces the surface tension between the water and air.[16−18] All measurements were conducted at room temperature.

Laser shadowography[19] was used to experimentally determine the equilibrium shape of the lenses. A schematic diagram of the optical system is shown in Figure 7. A shallow circular dish made of optical quality borosilicate glass with a depth of 2.5 cm and a diameter of 11.4 cm was filled with high purity water to a level of ≈0.5 cm from the top of the dish. A 100 μL hydrocarbon lens was deposited onto the surface of the water using a 100 μL precision

(15) Goebel, A.; Lunkenheimer, K. *Langmuir* **1997**, *13*, 369–372.
(16) Aveyard, R.; Cooper, P.; Fischer, P. D. I. *J. Chem. Soc., Faraday Trans.* **1990**, *86*, 3623–3629.
(17) Aveyard, R.; Binks, B. P.; Fletcher, P. D. I.; MacNab, J. R. *Langmuir* **1995**, *11*, 2515–2524.
(18) Aveyard, R.; Binksa, B. P.; Cooper, P.; Fletcher, P. D. I. *Adv. Colloid Interface Sci.* **1990**, *33*, 59–77.
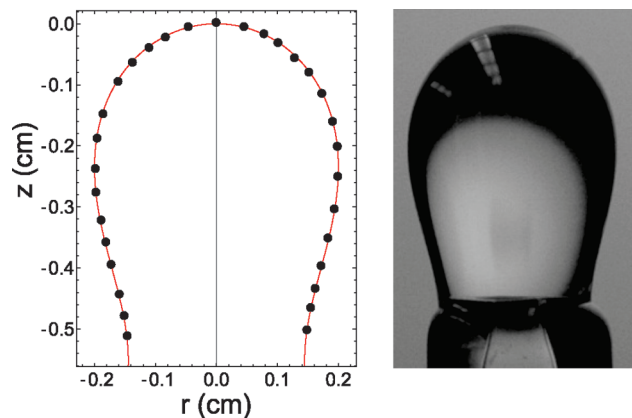(19) Nosoko, T.; Ohyama, T.; Mori, Y. H. *J. Fluid Mech.* **1985**, *161*, 329–346.

Figure 6. Image of a pendant water droplet hanging from a glass nozzle (right, rotated by 180 degrees). Points were manually chosen off of the profile of the drop and then fitted to solutions of eqs 3 and 4, using the contact angle at the nozzle and the surface tension as adjustable fitting parameters. Using this procedure, the surface tension of pure water at room temperature was measured to be 72.2 ± 0.4 dyn/cm.

Hamilton glass syringe, and then the dish was quickly covered with a 1.6 mm thick borosilicate glass plate. The cover prevented ambient air currents from moving the lens around the dish, and the cover also provided an enclosed environment which suppressed evaporation of the lens. For pure fluids, data were taken immediately following deposition of the lens. In experiments in which surfactants were purposefully introduced, the lenses were were left to equilibrate for 60 min before taking measurements. The dish containing the water and the floating lens was placed on a transparent horizontal platform on a vertically mounted optical rail so that its height could be precisely adjusted. A translucent paper screen with millimeter rulings was mounted in a fixed position on the optical rail above the dish. The camera (Nikon D70) with a macro lens was mounted ≈20 cm above the paper screen. The system was illuminated from below with green laser light (3 mW diode laser, 532 nm wavelength) that had been passed through a beam expander which provided a uniform beam of parallel rays approximately 4 cm in diameter. The hydrocarbon lens refracted the parallel beam into converging rays, as shown in Figure 7. Images of the lenses such as the one shown at the top of Figure 7 were obtained with a 6 megapixel digital camera. Digital photographs of the projected lens image were taken at a sequence of values of h, the distance between the screen and the flat surface of the water, at approximately 2 mm intervals.

In addition to the shadowgraphic technique, we also directly measured the contact angle γ of the water using Moiré imaging. The Moiré patterns and imaging method were nearly identical to those used by Dussaud et al.[20] which describes measurements of the deformation of a liquid surface with a spreading surfactant. In order to alter our experimental setup to accommodate the Moiré technique, a 2.5×2.5 cm^2 Ronchi ruling of pitch 127 μm was placed between the beam expander and the bottom of the dish, and the gridded screen was replaced with a second identical Ronchi ruling in contact with an identically sized piece of opal glass. The height of the second Ronchi ruling was adjusted until about 8 or 9 interference lines were visible. These lines were undeflected when no lens was present, confirming that the water was flat away from the perimeter of the dish (see Figure 10a). A 1 mL volume of unfiltered dodecane was placed on the water, and an image of the now deflected lines was taken (see Figure 10b). We tracked the deflection of the fringe line that would be perpendicular to the lens when undeflected, as Moiré lines deflect due to deformation along one axis only. For small values of γ, the total

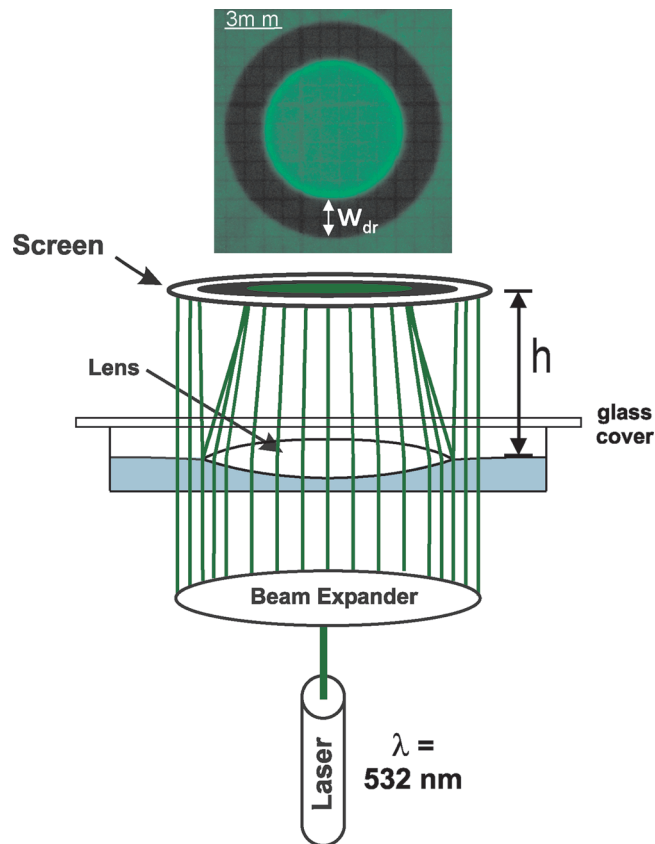(20) Dussaud, A. D.; Matar, O. K.; Troian, S. M. *J. Fluid Mech.* **2005**, *544*, 23–51.

Figure 7. Diagram of the experimental apparatus along with a typical image of an alkane lens. A 3 mW, 532 nm green diode laser was passed through a beam expander in order to produce uniform, planar illumination. The light passed through the water and liquid lens interfaces, where it is refracted. A gridded-screen was placed at variable heights above the lens in order to form an image, which was then photographed with a digital camera. The width of the dark ring in the photograph is denoted w_{dr}.

distance that a given line is deflected from far away from the lens (where the subphase surface is flat), up to the contact line, is proportional to the slope of the water's surface at the contact line, and thus the contact angle can be determined once the slope is known. A detailed description of the Moiré technique can be found in Patorski's book.[21]

Results

The accuracy and internal consistency of the entire numerical method was checked by measurements of pure hydrocarbon lenses of known volume on a pure water subphase. The simplest case involves partial wetting, where there is no microscopic hydrocarbon wetting layer on the water surface, which would presumably change the surface tension of the water/air interface. In this case, the seven known quantities are R, V, ρ_A, ρ_B, ρ_C, σ_{AC}, and σ_{BC}, which is enough to define a liquid lens system. The radius can be measured from the optical shadowgraphic images. We wish to determine the resulting spreading coefficient S from this configuration. However, the numerical technique requires S as an input, and the volume is an output. Thus, we adjusted the value of S in the numerical technique until the resultant lens volume V matched the known volume from the experimental lens (100 μL). Values obtained using this procedure are denoted as S_{exp} in Table 1. The error in the spreading coefficient for the pure alkane fluids

(21) Patorski, K. *Handbook of the Moiré Fringe Technique*; Elsevier: The Netherlands, 1993.

Table 1. Parameters Used and Measured in the Hydrocarbon Liquid Lens Systems[a]

fluid	ρ (g/cm^3)	σ_{oa} (dyn/cm)	R (cm)	S_{exp} (dyn/cm)	σ_{wa} (dyn/cm)
nonane	0.715	22.43	0.84	-0.73 ± 0.02	72.2
dodecane	0.745	24.94	0.60	-4.22 ± 0.19	72.2
tetradecane	0.758	26.15	0.56	-6.15 ± 0.30	72.2
hexadecane	0.728	23.41	0.65	-6.11 ± 0.15	72.2
mineral oil	0.862	29.19	0.54	-7.84 ± 0.49	57.8 ± 3.8

[a] The alkanes were filtered through a column of alumina powder to remove polar impurities, and in addition the dodecane and hexadecane were vacuum distilled. S was determined using the volume matching method outlined in the Results section. The error in S increases inverse to the lens radius, since changes in radii produce more pronounced changes in volume for fluids with large negative spreading coefficients. Oil/air surface tensions (denoted oa) and densities were taken from ref 14, except in the case of the mineral oil, for which the surface tension was measured using the axisymmetric drop shape technique outlined in the results section. The water/air surface tension (denoted wa) used was our measured value of 72.2 dyn/cm for pure water; however, in the case of mineral oil, σ_{wa} was used as an adjustable parameter due to suspected pseudopartial wetting.
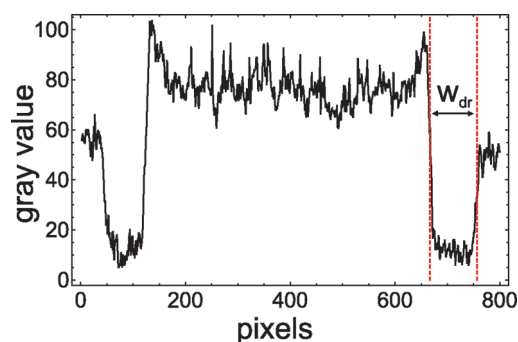

Figure 8. Plot of the optical intensity as a function of position across a diameter of a typical lens. Refraction produces a dark annular region of width w_{dr} surrounding a bright center region.

was dominated by the error in the radius measurements, so we computed the lens profile for the lower and upper bound on the radius, which gives upper and lower bounds on S_{exp}.

A plot of the intensity variation across a diameter is shown in Figure 8. The intensity variation has considerable structure which can be related to the shape of the lens, although it is sensitive to spatial variations in the illumination intensity. One of the most prominent features of the images is a dark ring formed by the refraction of the rays near the contact line. The width of the dark ring w_{dr} is a simple, robust, and model-independent feature that we used to characterize the images. This was experimentally determined by manually measuring the outer and inner diameter of the dark ring in pixels, subtracting these diameters, and then dividing by two. Diameters were averaged over two orthogonal directions in order to reduce error. The width of the dark ring was then converted to centimeters using the grid spacing on the screen. Edges could be located on the images with a resolution of 5 pixels (0.01 cm).

There are two optical properties of the lens/water system that determine w_{dr}. The dominant contribution comes from the focusing of the light due to the lens shape. Another contribution is due to the fact that the surface of the water must be curved near the contact line, as seen in Figure 4. This results in a divergence of the light which makes the outer diameter of the lens larger as the screen is placed farther away from the lens. The angular divergence δ is given by the formula $\delta = \arcsin(n_w \sin(\gamma)/n_a) - \gamma$, where n_w (n_a) is the index of refraction of the water (air) and γ is
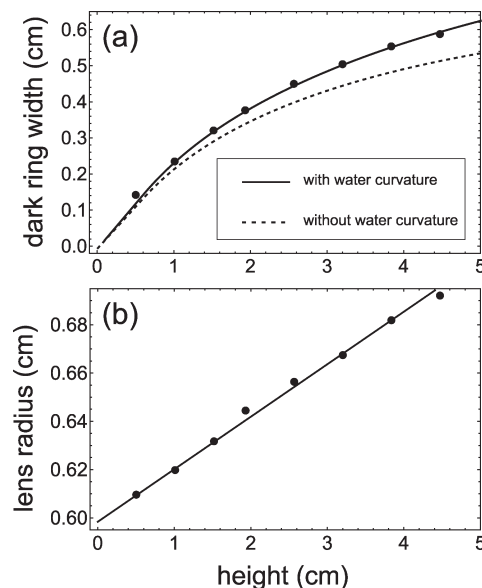

Figure 9. (a) Values of w_{dr} as a function of h for a 100 μL dodecane lens of radius 0.60 cm on water. The solid curve is the prediction obtained from ray-tracing through the computationally determined lens geometry. The dashed curve is the predicted behavior not including the effects of the water curvature near the contact line. (b) Radius of lens in the images as a function of height. The water curvature causes a slight divergence of the rays, which makes the radius of the lens appear larger for larger h. The solid line is a linear fit used to determine the actual radius of the lens.

the contact angle of the water at the contact line (see Figure 2). Although this divergence makes only a small correction to width of the dark ring w_{dr}, this term must be taken into account in order to obtain quantitative agreement with the experimental results (Figure 9). This divergence also affected the measurement of the radius of the lens. The radius was determined from shadowgraph images by measuring the outer diameter of the dark ring at different known heights h above the water surface. The apparent radius of the lens increases linearly with h because of the curvature of the water, so we fitted the apparent radius versus height to a line and extrapolated the results to zero height, which correspond to the true radius of the lens (Figure 9). Errors in the radius were dominated by the blurring of the edge of the lens image on the ruled paper and were of order ≈0.05 cm. The Moiré imaging independently confirms the predicted curved profile of the water. As shown in Figure 10, the water contact angle at the edge of a 1 mL dodecane lens of radius 1.57 cm was determined to be 3.6° ± 0.6° using the Moiré technique compared to a value of 3.69° predicted using the numerical method.

Once the lens profile was calculated using the numerical method, initially parallel light rays were traced through the oil/water, oil/air, and water/air interfaces using Snell's law so that w_{dr} could be found at a given distance from the lens. An example of this type of analysis is illustrated in Figure 12, which shows computed interfacial profiles for a tetradecane lens with volume 100 μL and radius 0.56 cm together with the refracted ray trajectories. The profile of the lens is compatible with the shape of oil lenses previously photographed in other studies.[22] The width of the ring where no light rays intersected the image plane and the intensity was nearly zero defines w_{dr}. This value was calculated as a function of height above the lens h, and compared to the shadowgraphy data as shown in Figure 9. Our initial attempts

(22) Boniewicz-Szmyt, K.; Pogorzelski, S.; Mazurek, A. *Oceanologia* **2007**, *49*, 413–437.
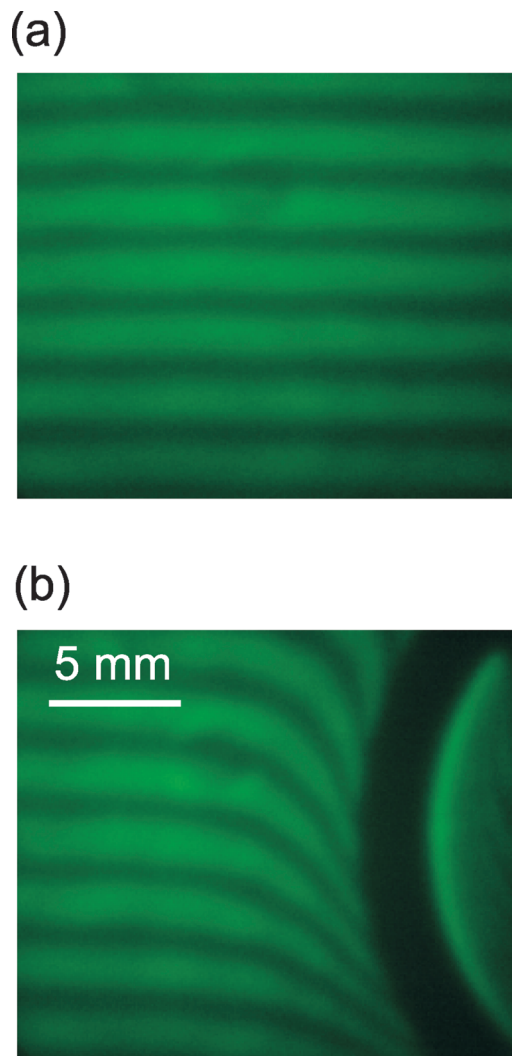
(a)

(b)

5 mm

Figure 10. (a) Moiré fringe lines of the surface of water at the center of a borosilicate glass dish with diameter 11.4 cm and height 0.6 cm. The lines are parallel and undeflected, indicating the surface of the water is flat. (b) Moiré fringe lines of the surface of water in the presence of an unfiltered dodecane lens 1.57 cm in radius. The deflection of the lines from their position without the lens presence is proportional to the angle of curvature of the water at the lens' edge.

to fit the data included only the optical effects of the lens itself, and ignored the curvature of the water subphase. Although the computed slope of the water near the contact line was only a few degrees, we found that including this effect produced substantial changes in the predicted values of w_{dr} (Figure 9). In fact, if the curvature of the water was neglected, there was typically no value of S which provided a consistent description of the radius, volume, and the variation of w_{dr} with h. The numerical calculation of w_{dr} versus h including the effects of water curvature and the experimental shadowgraphy data for mineral oil, tetradecane, dodecane, and nonane are shown in Figure 11. There are no free parameters in the predicted curves, and the agreement is excellent, which verifies the ray tracing method and the numerical method simultaneously. We should also note that when the light rays pass through the glass cover on the dish, they are slightly shifted in the horizontal direction due to refraction, and this was also taken into account, although the correction is rather small, and is negligible for a very thin glass cover.

In the case of mineral oil, we found that an accurate fit to the dark ring data could not be found simply by varying S with the
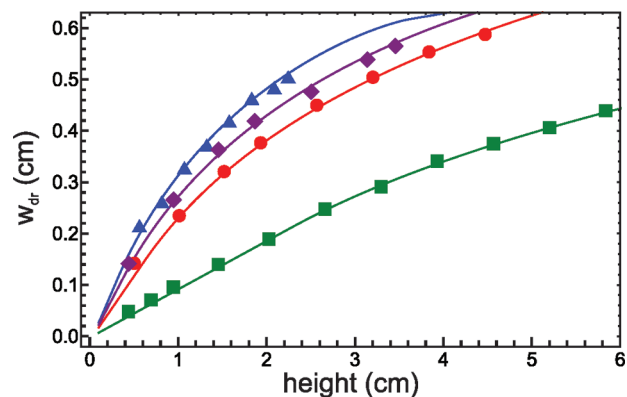

Figure 11. Values of w_{dr} obtained from 100 μL lenses of mineral oil (triangles), tetradecane (diamonds), dodecane (circles), and nonane (squares). The parameters associated with the lenses can be found in Table 1. The solid lines are the computed dark ring curves from the numerical and ray-tracing technique. The surface tension of the subphase was fixed at 72.2 dyn/cm, as it should be for pure water (except in the case of mineral oil, see the text for details). There are no fitting parameters involved in the generation of the theoretical solid curves for the alkanes.
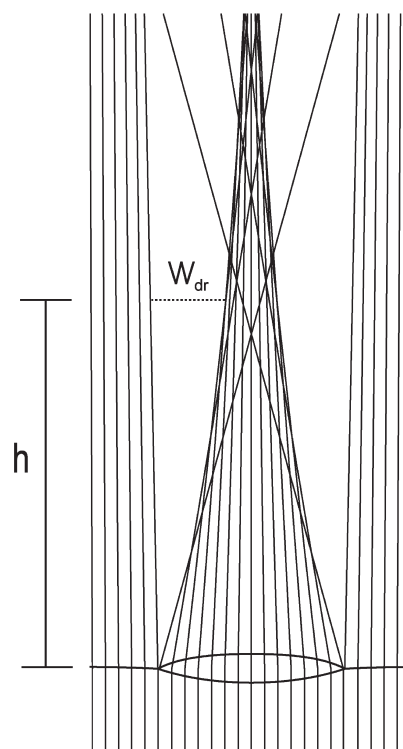

Figure 12. Computed geometry of 100 μL tetradecane lens of radius 0.56 cm with spreading coefficient -6.15 dyn/cm. Initially parallel rays from below are refracted by the liquid lens and the subphase. The region containing no rays corresponds to the black ring of Figure 7. The width of the dark region w_{dr} depends on the height of observation h. Measurements were always performed for values of h below which the rays begin to cross into the dark ring region (i.e., inside the focal length of the lens).

surface tension of the water/air interface fixed at its nominal value of 72.2 dyn/cm; considerably smaller values were required to fit the data. This is not surprising considering that the mineral oil was not purified (in contrast to the alkanes), so that impurities and surfactants are likely to be present. This could stabilize a thin layer of mineral oil on the surface of the water (pseudopartial wetting[5]), which would lower the water/air surface tension. In this case,
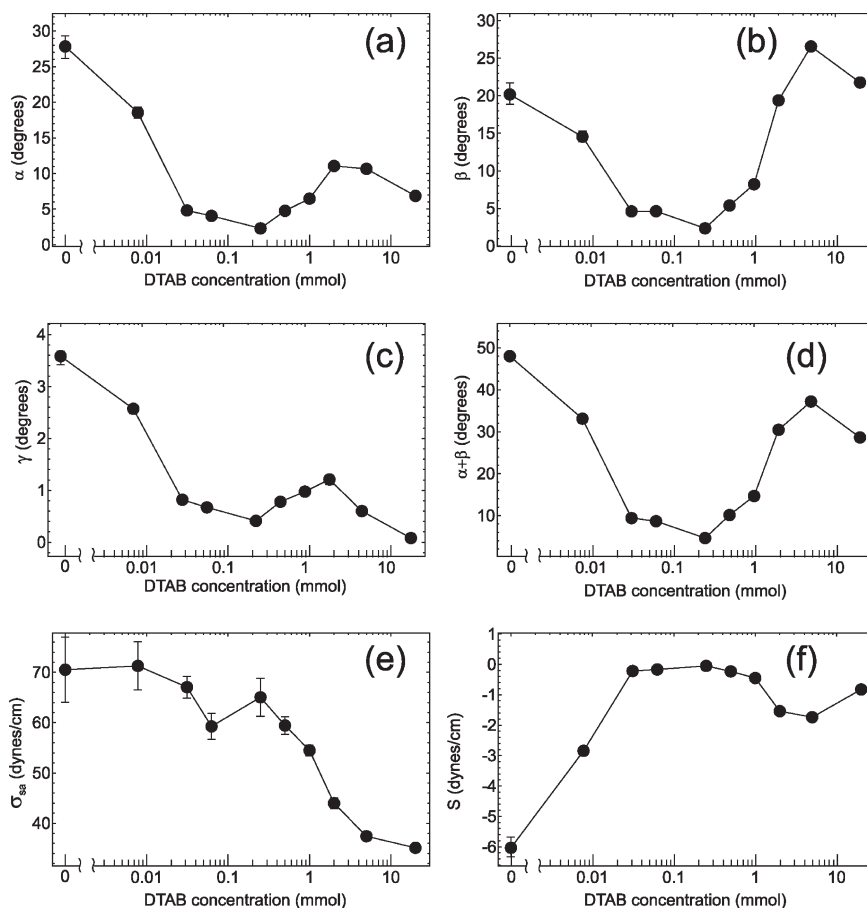
Figure 13. (a−c) Plot of the contact angles as defined in Figure 2 as a function of DTAB concentration in the aqueous subphase. The hexadecane lens becomes very flat around ≈0.25 mmol, so the contact angles become quite small. (d) The dihedral angle subtended by the lens is plotted in order to compare to data in Wilkinson et al.[13] (e-f) Plots of the subphase/air surface tension σ_{sa} and spreading coefficient S. The distinct dip in σ_{sa} at 0.25 mmol corresponds to the onset of the pseudopartial wetting transition, where a thin layer of hexadecane is solubilized onto the surface of the subphase. Although S is nearly zero, it is still negative, resulting in a finite-sized liquid lens.

we adjusted both the water/air surface tension and spreading coefficient to achieve a minimum in the χ^2 function associated with the fit, with the constraint that the volume of the lens be $100 \, \mu$L. The error in S was dominated by the 95% confidence interval in the parameter estimate, which we report in Table 1. Our values of the spreading coefficients are in qualitative but not quantitative agreement with prior experimentally measured values. Hirasaki[23] lists previous values for dodecane: −5.8 initially and −6.1 at equilibrium, both in dyn/cm. Langmuir[6] determines tetradecane has a spreading coefficient equal to −6.2 dyn/cm. Any discrepancies in these results are almost certainly due to variations in the purity of the fluids used, since small purity changes are known to result in fairly large fluctuations in the spreading coefficient.[24] We also observed substantial changes in S when a nominally (99+% pure) unfiltered dodecane lens was compared to dodecane purified using a column of alumina powder and/or vacuum distillation. Comparison of the measured and computed values for the width of the dark region provides a fairly convenient way of determining multiple unknown surface tensions, and all information about the lens geometry is known once a fit to the data is found.

To illustrate this point, we studied lenses using the hexane/water/DTAB system which has a well characterized transition to a pseudopartial wetting state[12,13] which can be controlled by the concentration of the surfactant DTAB. Lenses were measured on

aqueous solutions of purified water and DTAB with a range of concentrations from 0 to 20 mM. Figure 13 shows the various lens system parameters as a function of surfactant concentration in the subphase. The surfactant is not expected to change the hexadecane/air surface tension, which has the value 27.09 dyn/cm for all concentrations. The surfactant will however affect both the subphase/air interface and the hexadecane/subphase interface. As in the mineral oil case, the only known parameters are the lens radius and volume, fluid densities, and hexadecane/air surface tension, so both the spreading coefficient S and the subphase/air surface tension σ_{sa} must be determined. One constraint in the computation of the lens profiles is that the computed volume must match the known volume of the hexadecane lens ($100 \, \mu$L). For a given value of σ_{sa}, S was adjusted to meet this constraint. The value of σ_{sa} was used as a fitting parameter to match the measured dark ring width w_{dr} versus height h data at each concentration. Nonlinear regression analysis was used to compute the 95% confidence interval for the parameter estimates in σ_{sa} and S which determine the error bars associated with the data points.

As Figure 13 illustrates, the versatility in our method resides in the fact that once the best fit is computed, we know all the parameters in the system (e.g., contact angles α, β, γ). Consistent with Wilkinson et al.,[13] we see a minimum in the dihedral angle ($\alpha + \beta$) at a concentration of ≈0.25 mmol, which is attributed to the onset of the pseudopartial wetting regime (Figure 1b). This corresponds to a maximum in S, where S is very close to zero, but still negative so that the subphase is not completely wetted.

(23) Hirasaki, G. J. *J. Adhes. Sci. Technol.* **1993**, *7*, 285–322.
(24) Takii, T.; Mori, Y. H. *J. Colloid Interface Sci.* **1993**, *161*, 31–37.

Our results are in qualitative and semiquantitative agreement with previous results;[13] our measured values for the dihedral angle at concentrations above the pseudopartial wetting transition are significantly larger. This could be due to the fact that the DTAB surfactant was purified by recrystallization in Wilkinson et al.,[13] while we used unpurified surfactant as delivered by the manufacturer.

In conclusion, we have made detailed comparisons of optical measurements of various liquid lens systems with numerically determined equilibrium shapes. Our numerical method which solves the Young−Laplace equation has been implemented in *Mathematica*; the code is available in the Supporting Information, which also contains a free open source *Mathematica Player* file. For given values of the fluid densities, surface tensions, and the radius of the lens, the *Player* version of the Young−Laplace solver will output a graphical image of the lens and subphase, and numerical values of the contact angles and the volume of the lens, while the full version will also output a list of coordinates which define the interfaces of the lens. A comparison of observed and computed features of the lens provides a convenient method for measuring the spreading coefficient S and the effective water/air surface tension σ_{wa}. For purified fluids which are known to be free of surfactants, the literature value of σ_{wa} can be used, so S is the only unknown parameter. In this case, a single measurement of the radius and the volume of a lens is sufficient to determine S: the value of S can be varied in the Young−Laplace solver until the observed relation between radius and volume is achieved. In general, however, the properties of a liquid lens system can be significantly altered by the presence of even trace amounts of a surfactant which may be intentionally included or may exist as a contaminant. This results in a pseudopartial wetting film, which generally reduces the effective value of σ_{wa}. At least two independent measurements are required to determine the two values S and σ_{wa}. In principle, if sufficient sample fluid is available, the required data could be obtained from measurements of the radius and volume of lenses with a wide range of volumes. Optical measurement of the radius is complicated by the curvature of the subphase near the contact line, which we have quantitatively determined using Moiré imaging. Measurements of the shadow of a lens as a function of height above the subphase extrapolated back to zero height provide a precise method of determining the radius. Similarly, the width of the dark ring in the shadow as a function of height is an easily measured and robust feature of the optical image which can be obtained for a single lens. We have used this type of data to determine S and σ_{wa} for a variety of systems. This is accomplished by computing candidate lens profiles and tracing rays through them to find the width of the dark ring as a function of height, and then adjusting S and σ_{wa} to match the measured values. We have verified the effectiveness of this procedure for both pure fluids and systems containing surfactants.

Supporting Information Available: Free *Mathematica Player* file (Lens_Profiler, si_002) that can be used to compute the shapes of liquid lens systems. In addition, a full *Mathematica* file (Lens_Profiler_full, si_003) that can be used to export the data associated with the computed lens interfaces. This material is available free of charge via the Internet at http://pubs.acs.org.